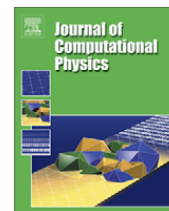




Contents lists available at ScienceDirect

## Journal of Computational Physics

journal homepage: [www.elsevier.com/locate/jcp](http://www.elsevier.com/locate/jcp)

## Compensated optimal grids for elliptic boundary-value problems

F. Posta<sup>a,1</sup>, S.Y. Shvartsman<sup>b</sup>, C.B. Muratov<sup>a,\*</sup><sup>a</sup> Department of Mathematical Sciences, New Jersey Institute of Technology, University Heights, Newark, NJ 07102, USA<sup>b</sup> Department of Chemical Engineering and Lewis Sigler Institute for Integrative Genomics, Princeton University, Princeton, NJ 08544, USA

## ARTICLE INFO

## Article history:

Received 7 December 2007

Received in revised form 19 May 2008

Accepted 12 June 2008

Available online 3 July 2008

## Keywords:

Finite-differences

Dirichlet-to-Neumann map

Rational approximation

Higher-order schemes

Cell communication

## ABSTRACT

A method is proposed which allows to efficiently treat elliptic problems on unbounded domains in two and three spatial dimensions in which one is only interested in obtaining accurate solutions at the domain boundary. The method is an extension of the optimal grid approach for elliptic problems, based on optimal rational approximation of the associated Neumann-to-Dirichlet map in Fourier space. It is shown that, using certain types of boundary discretization, one can go from second-order accurate schemes to essentially spectrally accurate schemes in two-dimensional problems, and to fourth-order accurate schemes in three-dimensional problems without any increase in the computational complexity. The main idea of the method is to modify the impedance function being approximated to compensate for the numerical dispersion introduced by a small finite-difference stencil discretizing the differential operator on the boundary. We illustrate how the method can be efficiently applied to nonlinear problems arising in modeling of cell communication.

© 2008 Elsevier Inc. All rights reserved.

## 1. Introduction

Many nonlinear problems in a broad range of applications in science and engineering lead to models which consist of coupled compartments of different spatial dimensionality (see e.g. [1–7]). For example, in many cell communication systems signaling molecules are emitted, interact with, and induce responses through the surfaces of cells forming a two-dimensional layer of epithelium while diffusing through the three-dimensional extracellular medium surrounding the epithelial layer [8] (for more details on this example, see the following section). Model formulation in such problems is complicated by the need, in general, to consider partial differential equations (PDEs) defined on two-dimensional surfaces (or even one-dimensional curves) in addition to the usual three-dimensional equations in the bulk. This mixture of spatial dimensions, especially on unbounded domains, naturally complicates the computational studies of these models.

Often in such problems, however, the equation in the bulk can be a simple linear PDE, as, e.g., in the case of the cell signaling example mentioned above where the concentration of the signaling molecule in the extracellular medium can be assumed to satisfy the diffusion equation in free space with some effective diffusion constant. In these cases it is possible to reduce the dimensionality of the problem via a boundary integral formulation. At the same time, such a formulation suffers from spatial (as well as temporal in the case of evolution problems) nonlocality which, once again, generally makes numerical studies of such problems difficult (for various approaches to this type of problems, see e.g. [9–14]).

A new approach to computing boundary data for linear second-order problems has been developed over the last decade which utilizes the concept of “optimal grids” [15–19]. This method applies a finite-difference discretization to the second-order elliptic operator, using a judiciously chosen sequence of unequal steps to accurately approximate the Neumann-to-

\* Corresponding author. Tel.: +1 973 596 5833; fax: +1 973 596 5591.

E-mail addresses: [fp2@njit.edu](mailto:fp2@njit.edu), [filippoposta@biomath.ucla.edu](mailto:filippoposta@biomath.ucla.edu) (F. Posta), [stas@princeton.edu](mailto:stas@princeton.edu) (S.Y. Shvartsman), [muratov@njit.edu](mailto:muratov@njit.edu) (C.B. Muratov).

<sup>1</sup> Present address: Department of Biomathematics, David Geffen School of Medicine, UCLA, Los Angeles, CA 90095-1766, USA.

Dirichlet (NtD) map associated with that operator in a number of simple geometries. The optimality of the approximation (in the sense which will be discussed in more detail in the following sections) allows to dramatically reduce the number of grid points in the direction normal to the boundary, making the dimensionality of the computational problem essentially equal to that of the boundary. This method has many advantages which make it a natural choice for the numerical studies of non-linear problems [20]. In particular, the method is second order-accurate in the size of spatial discretization of the boundary, and the size of the optimal grid can be chosen to match its accuracy with that of the finite-difference stencil on the boundary for all scales of the problem. When very high accuracy of the solution is not required, this approach results in very compact finite-difference approximation schemes for the original PDEs which are typically adequate for computational purposes.

Apart from increasing the size of the finite-difference grid, the most straightforward way to increase the accuracy of the optimal grid discretization would be to use a higher-order discretization for the transverse part of the differential operator in the bulk. This would increase the size of the stencil and naturally reduce the efficiency of the method. It appears, however, that the optimal grid method has the capacity for increasing the degree of accuracy of the obtained numerical solution on the boundary *without* increasing the size of the discretization stencil. Instead of resorting to higher-order stencils, one can attempt to modify the impedance function (for technical details see the following sections) in a way that it compensates for the numerical dispersion introduced by a small nearest-neighbor stencil. The obtained method, which we term the method of “compensated” optimal grids, is the subject of the present paper. We will illustrate this method with a number of examples in two- and three-dimensional elliptic boundary-value problems relevant to cell communication models. In particular, we will show that for two-dimensional problems on uniform grids along the boundary one could go from second-order to essentially spectral accuracy without increasing the computational complexity of the problem, while in three dimensions one can go from second- to fourth-order accurate method by either utilizing hexagonal lattices on the boundary or using a special 9-point stencil on square lattices.

Our paper is organized as follows. In Section 2, we give a motivating example from modeling cell communication by diffusing ligands. In Section 3, we review the method of optimal grids and introduce the idea of compensated optimal grids. Later on in this section we verify our method for a linear and an exactly solvable nonlinear problem. Then, in Section 4 we discuss ways to extend the two-dimensional version of the compensated optimal grids method to three dimensions. In Section 5, we present an application of our computational approach to a three-dimensional problem arising in cell communication modeling. Finally, in Section 6 we summarize our results.

## 2. Motivating example

We begin by discussing a typical example of a modeling setting in which the numerical issues discussed in this paper arise naturally [4]. Consider an idealized situation in which a flat epithelial layer is imbedded in a semi-infinite layer of extracellular medium (ECM), see Fig. 1. Cells at the bottom of the layer emit various signaling molecules which can then diffuse in the extracellular space and bind to their specific cell-surface receptors [8,22]. Binding of the signaling molecule to its respective receptor, in turn, activates the intracellular signaling cascades which elicit multiple cellular responses. Importantly, such responses may further regulate secretion of the acting signaling molecule, resulting in the establishment of positive and negative feedbacks [23].

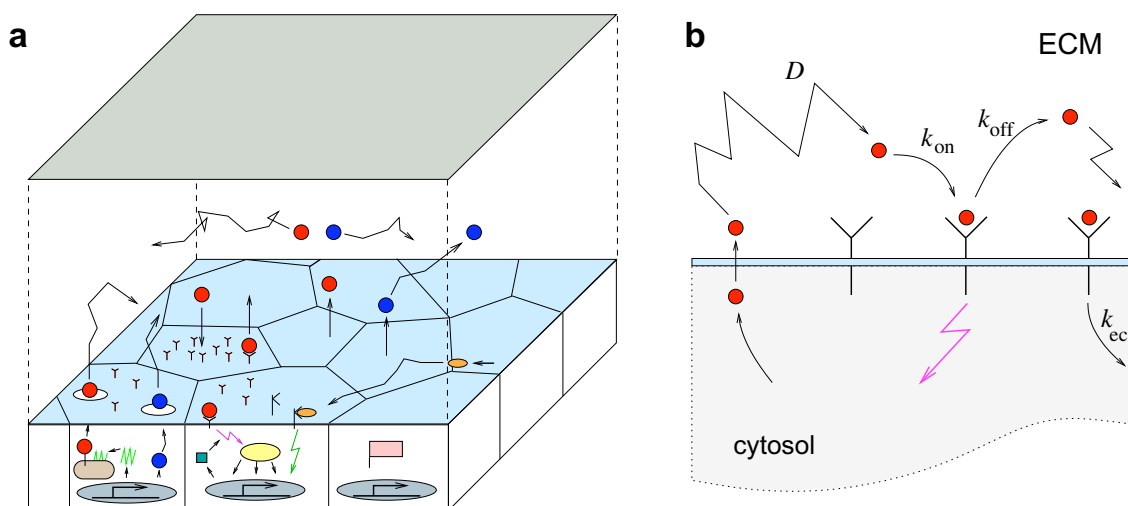


**Fig. 1.** The schematics of cell-to-cell signaling in an epithelial layer: the geometry of the epithelial layer (a) and the summary of the physical processes at the cell surface (b). In (a), red and blue circles show signaling molecules that are secreted by the epithelial cells, orange ovals represent the molecules of an imposed morphogen gradient. Both the signaling molecules and the morphogen bind to their specific cell-surface receptors, initiating responses by the intracellular machinery, represented by various symbols within cells. Details are taken from the signaling circuitry involved in the *Drosophila* egg development [21]. (For interpretation of the references in colour in this figure legend, the reader is referred to the web version of this article.)

In a mechanistic model of cell communication system the concentration  $s = s(t, x, y, z)$  of a signaling molecule in the ECM, chosen to occupy the upper half-space  $z > 0$ , satisfies the diffusion equation, together with an inhomogeneous Neumann boundary condition at the epithelium surface located at  $z = 0$ :

$$s_t = D_s \Delta s, \quad -D_s s_z|_{z=0} = g_s(t, x, y, s(t, x, y, 0)), \tag{1}$$

where  $\Delta = \partial_x^2 + \partial_y^2 + \partial_z^2$  denotes the three-dimensional Laplacian and  $g_s$  is the rate with which the signal is secreted from the unit area of the epithelium surface. Note that  $g_s$  can depend on the concentration of the signal itself on the cell surfaces, resulting in a direct feedback. More complex feedbacks may also arise via interaction with other molecular species, for simplicity we lump the effect of all these other species into an explicit dependence of  $g_s$  on time and position at the epithelium surface.

To see how a direct feedback may arise, consider the process of association of the signaling molecule (ligand) with its cell surface receptor into a ligand–receptor complex (see Fig. 1(b)) in the case of a simple autocrine relay [4,24,25]. Denoting by  $s^* = s^*(t, x, y)$  the surface density of the ligand–receptor complexes, we have the following equation for the ligand–receptor binding kinetics:

$$s_t^* = k_{s,on} r_s s(t, x, y, 0) - (k_{s,off} + k_{s,ec}) s^*, \tag{2}$$

where  $k_{s,on}$  is the forward ligand binding constant,  $r_s$  is the surface density of unoccupied receptors, assumed to be constant,  $k_{s,off}$  is the ligand–receptor dissociation constant, and  $k_{s,ec}$  is the rate of receptor-mediated endocytosis. The flux of the ligand across the cell membrane is, in turn,

$$g_s = -k_{s,on} r_s s(t, x, y, 0) + k_{s,off} s^* + \frac{\bar{g}_s s^{*\nu}}{s_0^{*\nu} + s^{*\nu}}, \tag{3}$$

where we assumed that the secretion rate of the ligands is a Hill (sigmoidal) function of the ligand–receptor complex density with Hill coefficient  $\nu$ , maximum secretion rate  $\bar{g}_s$  and threshold  $s_0^*$ , and treated the epithelium as a continuum two-dimensional homogeneous medium. Further invoking a biophysically reasonable approximation [4,24] of fast ligand–receptor binding kinetics (which is also exact for stationary solutions), we arrive at the following simplified expression for  $g_s$  which explicitly depends on the Dirichlet data  $s(t, x, y, 0)$  at the epithelium surface:

$$g_s = -\frac{k_{s,ec} k_{s,on} r_s s(t, x, y, 0)}{k_{s,off} + k_{s,ec}} + \frac{\bar{g}_s s^\nu(t, x, y, 0)}{s_0^\nu + s^\nu(t, x, y, 0)}, \tag{4}$$

where  $s_0$  is the appropriately rescaled threshold  $s_0^*$ . Note that for certain choices of the parameters the right-hand side in (4) is a cubic-like function, which results in the potential bistability of the considered signaling system [4,25]. In particular, in this case the stationary solutions of the problem satisfy

$$\Delta u = 0 \quad \text{for } z > 0, \quad u_z + f(x, y, u) = 0 \quad \text{at } z = 0, \tag{5}$$

where  $u$  and  $f$  are appropriately rescaled versions of the time-independent solutions for  $s$  and  $g$ , respectively, with  $f$  being a cubic-like function in the  $u$ -variable.

It is easy to see that to find solutions of (5), it is sufficient to solve for the trace  $\bar{u} = \bar{u}(x, y) \stackrel{\text{def}}{=} u(x, y, 0)$  of  $u$  on the epithelium surface. The latter, in turn, satisfies (see e.g. [26,20]):

$$\mathcal{A}\bar{u} + f(x, y, \bar{u}) = 0, \tag{6}$$

where  $\mathcal{A}$  is the Dirichlet-to-Neumann (DtN) map, a pseudo-differential operator whose action on plane waves is defined as:

$$\mathcal{A}e^{iq_1 x + iq_2 y} = -(q_1^2 + q_2^2)^{1/2} e^{iq_1 x + iq_2 y}. \tag{7}$$

Note that in some sense this equation can be thought of as one of the most natural nonlocal generalizations of the stationary reaction–diffusion equation

$$\Delta u + f(x, y, u) = 0. \tag{8}$$

The latter, in fact, also arises in the modeling of cell communication problems in another extreme when the signaling molecules are allowed to diffuse only in a narrow layer of ECM adjacent to the epithelium [24].

In the following, we show how the optimal grid method can be modified to serve as an alternative to the pseudospectral approach for solving problems like (6) numerically and can be used to obtain the solution with the accuracy comparable to that of pseudospectral methods. The latter is achieved via a suitable approximation of the DtN map by compact finite-difference operators.

### 3. Compensated optimal grids in two dimensions

In this section, we first review the main ideas of the application of the optimal grid method to elliptic problems and then introduce the method of compensated optimal grids in the simplest case of two-dimensional problems discretized on uniform grids in the transverse direction.

### 3.1. Optimal grid approach for the Laplace's equation in half-space

The method of optimal grids applied to (5) takes advantage of the fact that the DtN map  $\mathcal{A}$  can be, at least formally, thought of as the (negative) square root of the negative Laplacian operator restricted to the  $xy$ -plane [16]:

$$-\mathcal{A} = (-\mathcal{A}_\perp)^{1/2}, \quad \mathcal{A}_\perp = \partial_x^2 + \partial_y^2. \tag{9}$$

It then aims to approximate the square root function appearing in (9) by a rational function which arises as an impedance function of a staggered three-point finite-difference scheme used to approximate the boundary-value problem obtained by Fourier-transforming (5).

More precisely, applying Fourier transform to (5), we obtain the following equation for  $\hat{u}_\mathbf{q}(z) = \int_{\mathbb{R}^2} e^{iq_1x+iq_2y}u(x,y,z) dx dy$ , with  $\mathbf{q} = (q_1, q_2)$ :

$$\hat{u}_\mathbf{q}'' - \lambda_\mathbf{q}\hat{u}_\mathbf{q} = 0, \quad \lambda_\mathbf{q} = |\mathbf{q}|^2, \quad \hat{u}_\mathbf{q}'(0) = -\hat{f}_\mathbf{q}, \quad \hat{u}_\mathbf{q}(\infty) = 0. \tag{10}$$

Its solution at  $z = 0$ , which we are interested in, is given by

$$\hat{u}_\mathbf{q}(0) = F(\lambda_\mathbf{q})\hat{f}_\mathbf{q}, \quad F(\lambda) = \frac{1}{\sqrt{\lambda}}, \tag{11}$$

consistent with (6). The function  $F$  in (11) is the so-called impedance function of the corresponding continuous problem.

We now write the three-point staggered scheme in place of the second derivative in (10):

$$\frac{1}{h_k} \left( \frac{\hat{u}_\mathbf{q}^{k+1} - \hat{u}_\mathbf{q}^k}{h_{k+1/2}} - \frac{\hat{u}_\mathbf{q}^k - \hat{u}_\mathbf{q}^{k-1}}{h_{k-1/2}} \right) - \lambda_\mathbf{q}\hat{u}_\mathbf{q}^k = 0, \quad k = 1, 2, \dots, n-1, \tag{12}$$

$$\frac{\hat{u}_\mathbf{q}^1 - \hat{u}_\mathbf{q}^0}{h_{1/2}} - h_0\lambda_\mathbf{q}\hat{u}_\mathbf{q}^0 = -\hat{f}_\mathbf{q}, \quad \hat{u}_\mathbf{q}^n = 0. \tag{13}$$

Then we have  $\hat{u}_\mathbf{q}(0) \approx \hat{u}_\mathbf{q}^0$ , where

$$\hat{u}_\mathbf{q}^0 = F_n(\lambda_\mathbf{q})\hat{f}_\mathbf{q}, \tag{14}$$

provided that the impedance function

$$F_n(\lambda) = \frac{1}{\lambda h_0 + \frac{1}{h_{1/2} + \frac{1}{\lambda h_1 + \dots + \frac{1}{h_{n-1/2}}}}} \tag{15}$$

of the discrete problem, obtained by setting  $F_n(\lambda_\mathbf{q}) = \hat{u}_\mathbf{q}^0$  with  $\hat{f}_\mathbf{q} = 1$  in (12) and (13), is sufficiently close to the impedance function  $F(\lambda)$  of the continuous problem on a suitable spectral interval  $\lambda \in [\lambda_{\min}, \lambda_{\max}]$  [17,15,16].

The optimality of the obtained discretization scheme refers to such a choice of the discretization steps  $h_k$  which makes the approximation of  $F(\lambda)$  by  $F_n(\lambda)$  best in some sense on the prescribed spectral interval. A particularly good choice of the optimality criterion which leads to the so-called Zolotarev grids is to minimize the sup-norm of the relative error in approximating  $F$  with  $F_n$ :

$$\max_{\lambda \in [\lambda_{\min}, \lambda_{\max}]} \left| \frac{F_n(\lambda)}{F(\lambda)} - 1 \right| = \min_{\tilde{F}_n} \max_{\lambda \in [\lambda_{\min}, \lambda_{\max}]} \left| \frac{\tilde{F}_n(\lambda)}{F(\lambda)} - 1 \right|, \tag{16}$$

where the trial functions  $\tilde{F}_n$  are chosen among all rational functions of order  $n - 1$  by  $n$ . It was proved by Ingerman, Druskin and Knizhnerman that such an approach always produces an optimal rational approximant  $F_n$  of the impedance function in (11) for which all  $h_k > 0$ , a necessary condition for the stability of such a scheme [16]. Moreover, this approach demonstrates exponential superconvergence in the number of discretization nodes  $n$ .

When Fourier-transformed back to the real space, the method presented above becomes a semi-discrete approximation of the boundary-value problem in (5) [20]. In practice, the transverse Laplacian  $\mathcal{A}_\perp$  is then further approximated by some compact finite-difference stencil, the resulting fully discrete problem can be then analyzed using any standard method for finite-difference schemes.

### 3.2. Basic idea of compensation

In a practical implementation of the optimal grid method the use of the finite-difference stencil for approximating the transverse part of the differential operator introduces a source of error that is distinct from the error of the rational approximation of the impedance function and cannot be as easily controlled. We illustrate this point by considering a canonical problem of the Laplace's equation on half-plane. Consider plane wave solutions of (5) which do not depend on  $y$ :

$$u(x,z) = \frac{1}{q} e^{iqx - qz}, \quad f = e^{iqx}, \quad q > 0. \tag{17}$$

Now suppose one discretizes this problem on a cartesian product of a Zolotarev grid in the  $z$ -direction and a uniform grid with step size  $h_{\perp}$  in the  $x$ -direction, and uses a standard three-point central difference to approximate  $\Delta_{\perp}$ . Then the solution in (17) at  $z = 0$  is approximated by

$$u(x, 0) \approx F_n(2h_{\perp}^{-2}(1 - \cos qh_{\perp}))e^{iqx}, \tag{18}$$

which is obtained from (14) by observing that in the considered situation the approximation of  $\Delta_{\perp}$  with the three-point finite-difference stencil amounts to the replacement of  $\lambda_q = q^2$  in (10) with  $\lambda_q = 2h_{\perp}^{-2}(1 - \cos qh_{\perp})$  in (14). By choosing  $\lambda_{\max} = O(h_{\perp}^{-2})$  one can ensure that the rational approximant  $F_n$  resolves equally well all the high-frequency modes of the discrete problem, while adjusting the values of  $\lambda_{\min} = O(1)$  and  $n$  one can guarantee a specified accuracy of the rational approximation for a given range of wave vectors  $q$ . From this and the error estimate of [16] one can see that

$$qe^{-iqx}u(x, 0) = qF(2h_{\perp}^{-2}(1 - \cos qh_{\perp})) + O\left(e^{-\frac{\pi^2 n}{\ln h_{\perp}^{-1}}}\right), \tag{19}$$

i.e., the relative error of the considered finite-difference approximation to the solution in (17) is  $O(h_{\perp}^2) + O\left(e^{-\frac{\pi^2 n}{\ln h_{\perp}^{-1}}}\right)$ , with the first part of the error coming from the finite-difference approximation of  $\Delta_{\perp}$  and the second from the rational approximation of  $F$ . Thus, for  $n$  big enough the main source of error in (18) is, in fact, the numerical dispersion associated with the three-point stencil to approximate  $\Delta_{\perp}$ . On the other hand, observe that this numerical dispersion is passed on to the problem only in the form of the argument of the impedance function  $F_n$ , which in a practical implementation of the method essentially coincides with the impedance function  $F$  of the continuous problem on the considered spectral interval.

Our idea of compensation is to modify the impedance function  $F$  being approximated to cancel out the effect of the numerical dispersion associated with the finite-difference approximation of the transverse part of the differential operator. For the problem considered here one should, therefore, find a rational approximation  $F_n(\lambda) \approx F_c(\lambda)$  of the form of (15) with

$$F_c(\lambda) = \frac{h_{\perp}}{\arccos\left(1 - \frac{1}{2}\lambda h_{\perp}^2\right)}. \tag{20}$$

The choice of this function is determined by the requirement that the composition of  $F_c$  with  $\lambda_q$  gives the exact impedance function as a function of  $q$ , i.e., we have  $F_c(2h_{\perp}^{-2}(1 - \cos qh_{\perp})) \equiv F(q^2)$ , and the first error term arising in (19) has been completely eliminated. On the other hand, by choosing  $n$  sufficiently large one can efficiently control the accuracy of the approximation of  $F_c$  by  $F_n$  uniformly on the prescribed spectral interval, thus making the proposed numerical approach essentially spectrally accurate.

A natural question which arises in connection with the idea of compensation is how to choose an appropriate spectral interval. Obviously, for a problem discretized on a finite uniform grid of size  $m$  in the  $x$ -direction it is sufficient to choose

$$\lambda \in [\lambda_{\min}, \lambda_{\max}], \quad \lambda_{\min} = \frac{\pi^2}{m^2 h_{\perp}^2}, \quad \lambda_{\max} = \frac{4a^2}{h_{\perp}^2}, \tag{21}$$

with  $a = 1$ . Note, however, that it is not immediately obvious whether the impedance function  $F_c$  can be approximated on the spectral interval in (21) by a rational function of the form of (15) with all  $h_i > 0$ . In fact, this is questionable for  $a = 1$ , since the function  $F_c$  cannot be a Markov function [16], since it is not defined for  $\lambda > \lambda_{\max}$  in this case. On the other hand, for  $a \ll 1$  the function  $F_c$  essentially coincides with  $F$  on the spectral interval, hence by continuity the Zolotarev optimal rational approximant should be extendable to the function  $F_c$  as well. Therefore, for each  $n$  fixed it should be possible to approximate the compensated impedance function  $F_c$  on the spectral interval in (21) for some  $a < 1$  in a way which results in the optimal grid with positive steps.

We have implemented this approximation procedure for the impedance function  $F_c$  in (20), using Remez algorithm [27], and were able to generate optimal rational approximants for a broad range of values of  $m$  and  $n$ . For, example the (nearly) optimal rational approximant for  $F_c$  with  $h_{\perp} = 1$ ,  $n = 6$ ,  $m = 100$ , and  $a = 0.5$  on the interval from (21) is given by

$$F_n(\lambda) = \frac{0.0270636}{\lambda + 0.00203588} + \frac{0.0548426}{\lambda + 0.0113022} + \frac{0.120905}{\lambda + 0.0559717} + \frac{0.308876}{\lambda + 0.294184} + \frac{1.86027}{\lambda + 2.69169} + \frac{0.0166147}{\lambda + 0.00015466}, \tag{22}$$

where we found this value of  $a$  to be roughly the maximum value at which the algorithm converged to a solution with negative poles and positive residues. The relative error in approximating  $F_c$  in (20) on the spectral interval in (21) did not exceed  $1.2 \times 10^{-5}$  (see Fig. 2), showing the usual high performance of optimal grids [16]. Also, following the procedure of [20], we have extracted the grid steps from (22), these are given in Table 1 below.

Note that for fixed ratio of  $\lambda_{\max}$  to  $\lambda_{\min}$ , the grid steps corresponding to different values of  $h_{\perp}$  can be obtained from those with  $h_{\perp} = 1$  by a simple rescaling.

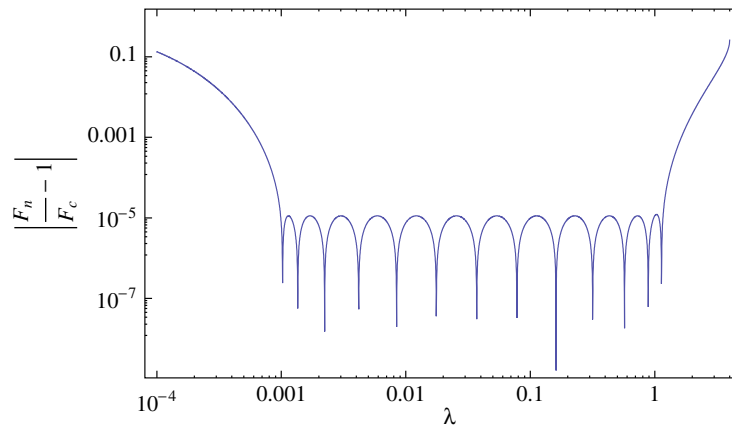


Fig. 2. The relative error in approximating  $F_c$  in (20) with  $F_n$  from (22).

**Table 1**  
The optimal grid steps corresponding to (22)

$h_0$	$h_{1/2}$	$h_1$	$h_{3/2}$	$h_2$	$h_{5/2}$
0.41866	1.11746	1.76275	2.61108	3.77355	5.44027
$h_3$	$h_{7/2}$	$h_4$	$h_{9/2}$	$h_5$	$h_{11/2}$
7.89149	11.5611	17.1795	26.1855	42.328	82.559

### 3.3. Comparison with Zolotarev and geometric optimal grids

We now compare performance of the compensated optimal grids constructed in the preceding section with that of the “uncompensated” Zolotarev and geometric optimal grids [16,20] of the same size applied to the plane wave solutions of the Laplace’s equation on half-plane. For the comparison purposes, we have implemented a discretized version of the boundary-value problem

$$\frac{\partial^2 u}{\partial x^2} + \frac{\partial^2 u}{\partial z^2} = 0 \quad \text{in } [0, \pi] \times [0, \infty), \quad \frac{\partial u}{\partial z} \Big|_{z=0} = -\cos qx, \quad \frac{\partial u}{\partial x} \Big|_{x=0,L} = 0, \quad (23)$$

where  $q = 1, 2, \dots$ , which reads

$$\frac{u_{j+1}^k - 2u_j^k + u_{j-1}^k}{h_{\perp}^2} + \frac{1}{h_k} \left( \frac{u_j^{k+1} - u_j^k}{h_{k+1/2}} - \frac{u_j^k - u_j^{k-1}}{h_{k-1/2}} \right) = 0, \quad k \geq 1, \quad (24)$$

$$\frac{u_{j+1}^0 - 2u_j^0 + u_{j-1}^0}{h_{\perp}^2} + \frac{1}{h_0} \left( \frac{u_j^1 - u_j^0}{h_{1/2}} + \cos qx_j \right) = 0, \quad x_j = jh_{\perp}, \quad (25)$$

with  $j = 0, 1, \dots, m$  and  $k = 0, 1, \dots, n - 1$ , the value of  $h_{\perp} = \pi/m$ , and the boundary conditions

$$u_{-1}^k = u_1^k, \quad u_{m+1}^k = u_{m-1}^k, \quad u_j^n = 0. \quad (26)$$

We solved (24)–(26) using the diagonally preconditioned conjugate gradient method with a number of different kinds of choices of  $h_k$ : compensated grids with  $n = 8$  and  $n = 10$  optimized on the spectral interval  $\left[ \frac{m^2}{10000\pi^2}, \frac{m^2}{10\pi^2} \right]$ , a compensated grid with  $n = 14$  optimized on the spectral interval  $\left[ \frac{m^2}{20000\pi^2}, \frac{m^2}{20\pi^2} \right]$ , optimal geometric and Zolotarev grids with different values of  $n$ , with Zolotarev grids optimized for the condition number  $\lambda_{\max}/\lambda_{\min} = 10^3$ ; both the geometric and the Zolotarev grids were scaled so that  $h_{1/2} = h_{\perp}$ . Note that the accuracy of the rational approximation for the compensated grids was  $6 \times 10^{-9}$  for  $n = 10$  and  $1.6 \times 10^{-12}$  for  $n = 14$ , while the accuracy of the Zolotarev’s approximation of the square root for  $n = 14$  was also found to be  $1.6 \times 10^{-12}$ .

We first ran a series of simulations for different values of  $q$  at fixed  $m = 1000$  and plotted the relative error of the solution. The results are presented in Fig. 3, where the left panel shows the comparison of the data obtained using compensated, geometric, and optimal grids with  $n = 8$ , while the right panel shows the same results with  $n = 14$ . Our first observation is that the performance of the geometric and Zolotarev optimal grids was not substantially improved with increasing the value of  $n$ . This is consistent with the arguments of Section 3.2 that the main source of error is the discretization of the transverse Laplacian, and not the rational approximation of the inverse square root. Our second observation is that in all cases the compensated optimal grids significantly outperformed the geometric and Zolotarev optimal grids. For  $n = 8$  the error in the solution

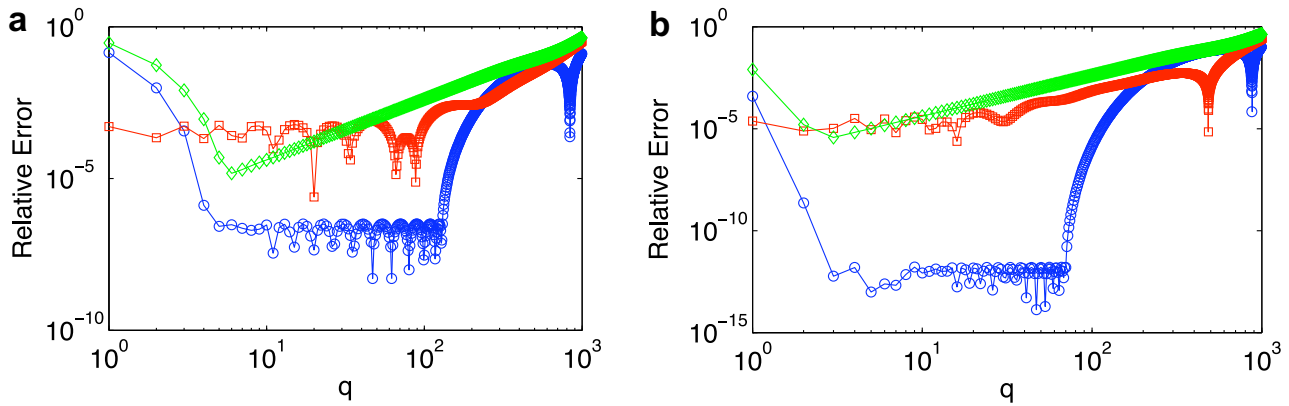


**Fig. 3.** Comparison of the performance of different optimal grids for solving the boundary-value problem in (23) with  $m$  fixed. In both (a) and (b), the relative error of the solution is shown for all admissible values of  $q$ ;  $n = 8$  in (a) while  $n = 14$  in (b). Red, green, and blue lines show the results of using geometric, Zolotarev, and compensated optimal grids, respectively. In all cases  $m = 1000$ . (For interpretation of the references in colour in this figure legend, the reader is referred to the web version of this article.)

did not exceed  $10^{-6}$ , while roughly doubling the size of the compensated optimal grid reduced the error down to about  $10^{-12}$  for essentially all wave vectors.

The performance of the grid deteriorates in two extremes: for large and for small wave vectors  $q$ . The discrepancy for large wave vectors is due to the fact that the spectral interval of optimization was chosen so that  $a \simeq 0.1$  in (21), thus the highest frequencies of the discrete problem were not completely resolved. On the other hand, the discrepancy at small wave vectors has to do with the resolution limit of the optimal grid set by the condition number of the optimization interval, for all the grids used in (3) this condition number was set to  $10^3$ . Note that similar deterioration in performance occurs also in the case of the Zolotarev grids because of the same nature of the approximation procedure. On the other hand, the geometric grid does slightly better at small wavevectors, since optimal geometric grids have a tendency to over-resolve low frequencies.

To further illustrate an essentially pseudo-spectral character of the accuracy of the compensated optimal grids, we performed a convergence study of the solution at fixed  $q$  as the value of  $m$  is increased. The results for  $q = 4$  and several choices of optimal grids are shown in Fig. 4. While the error of the geometric and Zolotarev grids shows the expected  $O(m^{-2})$  behavior, the error of the compensated optimal grid quickly falls to the value determined by the maximum resolution of the rational approximant. Once again, only when  $m$  exceeds a sufficiently large value at which the considered wavenumber goes outside of the interval of resolution, the error of the solution begins to grow.

We would also like to point out that the compensated optimal grids allowed us to achieve very high accuracy in approximating the solution by using grids of relatively small sizes. For example, the grid with just  $n = 10$  nodes already achieves single-precision accuracy for the range of  $m \sim 10 \times 10^3$  in the simulation of Fig. 4.

### 3.4. An exactly solvable nonlinear problem

We now apply the method presented in the preceding sections to a nonlinear problem admitting an exact solution. As was observed by Toland [28], for the following boundary-value problem

$$\frac{\partial^2 u}{\partial x^2} + \frac{\partial^2 u}{\partial z^2} = 0 \quad \text{in } \mathbb{R} \times [0, \infty), \quad \frac{\partial u}{\partial z} + \sin u = 0 \quad \text{on } z = 0, \tag{27}$$

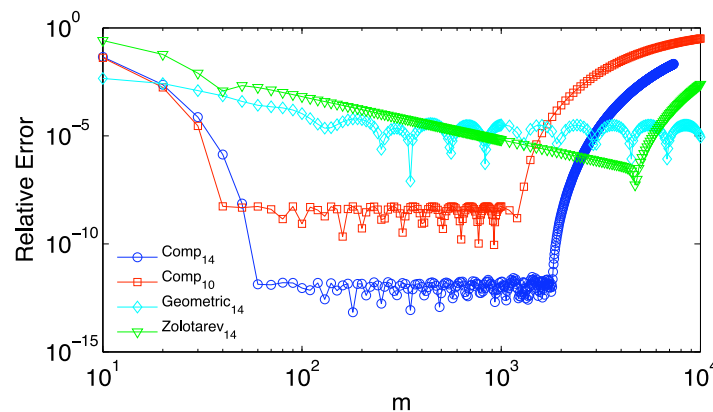


**Fig. 4.** Convergence study for the solution of (23) with  $q = 4$ . Results for the compensated grids with  $n = 10$  and  $n = 14$ , as well as geometric and Zolotarev grids with  $n = 14$  are shown.

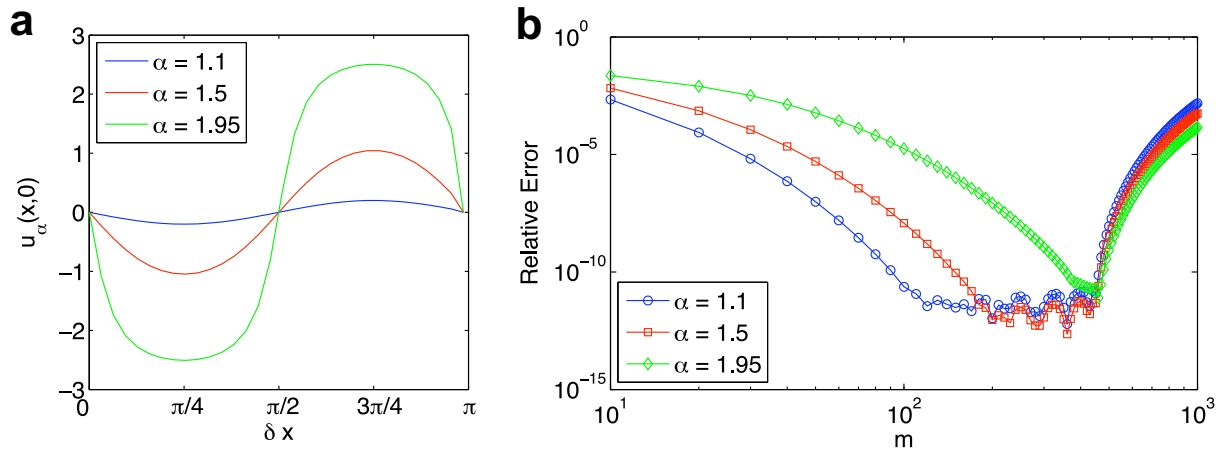


**Fig. 5.** (a) The form of the solutions of (27) for several values of  $\alpha$ . (b) Results of the convergence studies of the numerical solution using a compensated grid with  $n = 14$  obtained in Section 3.2.

all bounded solutions are  $(\pi/\delta)$ -periodic (the case of  $\delta \rightarrow 0^+$  corresponds to the Peierls front solution [29]), and at the line  $z = 0$  are given by a one-parameter family of functions (up to translations, reflections, and additions of multiples of  $2\pi$ )

$$u_x(x, 0) = 2\{\arctan(\gamma^{-1} \tan \delta x) - \arctan(\gamma \tan \delta x)\}, \quad \alpha \in (1, 2), \tag{28}$$

where

$$\beta = \alpha^2 - 2\alpha, \quad \delta = \frac{1}{2}\sqrt{-\beta}, \quad \gamma = \alpha/\sqrt{-\beta}. \tag{29}$$

The profiles of the solutions for several values of  $\alpha$  are shown in Fig. 5(a).

Fixing the value of  $\alpha$ , we discretized the problem on the domain  $[0, \frac{\pi}{2\delta}] \times [0, +\infty)$ , using the product of a uniform grid with  $m$  nodes and a compensated optimal grid with  $n = 14$  nodes obtained in Section 3.2 (suitably rescaled). Dirichlet boundary conditions were applied at the lateral boundaries. We then solved the obtained discrete problem numerically using a relaxation method by replacing the Laplacian in (27) with a diffusion operator and evolving the solution to the steady state from a suitably chosen initial condition. Namely, defining  $u_j^k(t)$  with  $t = 0, \Delta t, 2\Delta t, \dots$ , with  $\Delta t$  sufficiently small to ensure stability, we iterated the following scheme

$$\frac{u_j^k(t + \Delta t) - u_j^k(t)}{\Delta t} = \frac{u_{j+1}^k(t) - 2u_j^k(t) + u_{j-1}^k(t)}{h_\perp^2} + \frac{1}{h_k} \left( \frac{u_j^{k+1}(t) - u_j^k(t)}{h_{k+1/2}} - \frac{u_j^k(t) - u_j^{k-1}(t)}{h_{k-1/2}} \right), \quad k \geq 1, \tag{30}$$

$$\frac{u_j^0(t + \Delta t) - u_j^0(t)}{\Delta t} = \frac{u_{j+1}^0(t) - 2u_j^0(t) + u_{j-1}^0(t)}{h_\perp^2} + \frac{1}{h_0} \left( \frac{u_j^1(t) - u_j^0(t)}{h_{1/2}} + \sin u_j^0(t) \right), \quad u_j^n = u_0^k = u_m^k = 0, \tag{31}$$

until convergence to steady state. We then performed convergence studies in  $m$  as the value of  $m$  is increased. The results of this analysis for several values of  $\alpha$  are shown in Fig. 5(b). Here one can see once again that, as  $m$  increases, the  $L^\infty$  norm of the relative error of the obtained numerical solution drops down to the resolution limit of the compensated optimal grid. For example, for  $\alpha = 1.5$  increasing the size of the problem by a factor of 2 decreases the relative error by about an order of magnitude, until the error reaches the limit of about  $10^{-12}$ . As expected, further increase of the problem size does not produce any improvement of accuracy. Moreover, at some critical value of  $m$  the accuracy begins to deteriorate, since the optimal grid is no longer able to accurately treat long-wave Fourier modes. Note that the range of values of  $m$  for which the optimal accuracy of the method is achieved decreases as  $\alpha \rightarrow 2$ , i.e., when the profile of the solution becomes more and more front-like (see Fig. 5(a)). This is natural, since in this case one needs to accurately resolve more wavenumbers simultaneously, which puts constraints on the spectral radius used in the rational approximation.

To summarize these numerical studies, the method of compensated optimal grids applied to the considered nonlinear problem produces solutions that are essentially spectrally accurate. This is quite surprising for a finite-difference method based on a five-point stencil. Moreover, the method provides an easy way to control the error of the approximation and allows to obtain the solutions with high accuracy, using relatively small finite-difference grids.

#### 4. Extension to three-dimensional problems

We now show how the idea of compensation can be extended to the discretizations of three-dimensional problems. To illustrate our points, let us consider the following simple boundary-value problem

$$\frac{\partial^2 u}{\partial x^2} + \frac{\partial^2 u}{\partial y^2} + \frac{\partial^2 u}{\partial z^2} = 0 \quad \text{in } [0, L_x] \times [0, L_y] \times [0, \infty), \tag{32}$$

$$\left. \frac{\partial u}{\partial z} \right|_{z=0} = -\cos q_1 x \cos q_2 y, \quad \left. \frac{\partial u}{\partial x} \right|_{y=0, L_y} = 0, \quad \left. \frac{\partial u}{\partial y} \right|_{x=0, L_x} = 0, \tag{33}$$

where  $q_1$  and  $q_2$  are integer multiples of  $\pi/L_{x,y}$ , respectively. Unfortunately, the straightforward extension of the method of Section 3.2 to (32) and (33) which replaces the three-point stencil with a five-point centered difference for  $\Delta_\perp$  on a square grid with step  $h_\perp$  would not work because of the numerical anisotropy introduced by such a discretization. As a result, only the modes with either  $q_1 = 0$  or  $q_2 = 0$  would be accurately resolved, while one would still encounter an  $O(h_\perp^2)$  error when both  $q_1 \neq 0$  and  $q_2 \neq 0$ . We ran the solver using various combinations of  $q_1$  and  $q_2$  and the results obtained show that the one-dimensional compensated grid still performs no better than the geometric optimal grid of the same size (data not shown).

#### 4.1. Compensation on hexagonal grids

Alternatively, one may seek to discretize  $\Delta_\perp$  using a grid which possesses some extra degree of isotropy. The simplest such grid is, in fact, the hexagonal grid, provided one uses a 7-point stencil to approximate the transverse Laplacian. Hence, we discretize the problem as follows:

$$\frac{2}{3h_\perp^2} \sum_{j \in \mathcal{N}_j} (u_j^k - u_j^k) + \frac{1}{h_k} \left( \frac{u_j^{k+1} - u_j^k}{h_{k+1/2}} - \frac{u_j^k - u_j^{k-1}}{h_{k-1/2}} \right) = 0, \quad k \geq 1, \tag{34}$$

$$\frac{2}{3h_\perp^2} \sum_{j \in \mathcal{N}_j} (u_j^0 - u_j^0) + \frac{1}{h_0} \left( \frac{u_j^1 - u_j^0}{h_{1/2}} + \cos q_1 x_j \cos q_2 y_j \right) = 0, \tag{35}$$

where the index  $j$  denotes a point on the hexagonal grid of step size  $h_\perp$  contained inside a rectangle  $[0, L_x] \times [0, L_y]$  and aligned with its sides (see Fig. 6(a)),  $(x_j, y_j)$  denotes the cartesian coordinates of the point with index  $j$ , and  $\mathcal{N}_j$  is the set of 6 nearest neighbors of the  $j$ -th point. Reflecting boundary conditions are imposed on the rectangle boundaries, and a Dirichlet boundary condition at  $k = n$ . In practice, the discretization is performed using a general purpose code that we developed which combines finite volume discretization using Voronoi tessellation in the  $xy$ -plane with a staggered grid in the  $z$ -direction.

Observe that for the considered discretization in the plane we have

$$e^{-iq_1 x - iq_2 y} \Delta_\perp e^{iq_1 x + iq_2 y} \approx \frac{4}{3h_\perp^2} \left\{ \cos(q_1 h_\perp) + 2 \cos\left(\frac{q_1 h_\perp}{2}\right) \cos\left(\frac{q_2 h_\perp \sqrt{3}}{2}\right) - 3 \right\} = -|\mathbf{q}|^2 + \frac{1}{16} h_\perp^2 |\mathbf{q}|^4 + O(h_\perp^4), \tag{36}$$

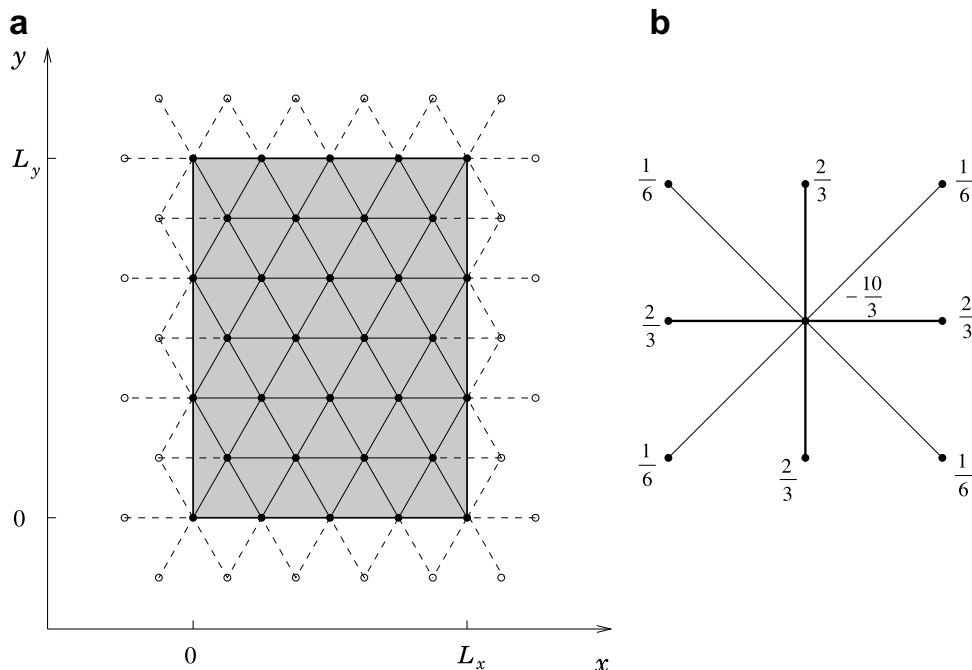


**Fig. 6.** (a) The discretization of the rectangular domain using a hexagonal grid. (b) The 9-point anisotropy-adjusted stencil for  $\Delta_\perp$  on a square grid. In (a), the solid circles show the discretization nodes, while the empty circles correspond to the ghost nodes of the reflecting boundary. Similarly, solid lines in (a) show the connections between the discretization nodes, while dashed lines show the connections to the ghost nodes. In (b), the fractions give, apart from the factor of  $h_\perp^{-2}$ , the weights of different nodes in the stencil.

where the last term in the last line depends explicitly on both  $q_1$  and  $q_2$ , while the first two depend only on the modulus  $|\mathbf{q}| = \sqrt{q_1^2 + q_2^2}$  of  $\mathbf{q} = (q_1, q_2)$ . So, since the discrete problem diagonalizes in the basis of plane waves with suitably chosen  $(q_1, q_2)$ , we have explicitly that

$$u(x_j, y_j, 0) \approx \cos q_1 x_j \cos q_2 y_j \times F_n \left[ \frac{4}{3h_\perp^2} \left\{ 3 - \cos(q_1 h_\perp) - 2 \cos\left(\frac{q_1 h_\perp}{2}\right) \cos\left(\frac{q_2 h_\perp \sqrt{3}}{2}\right) \right\} \right], \quad (37)$$

where  $F_n$  is the impedance function of the grid in the  $z$ -direction. The idea of compensation now is to modify the impedance function  $F$  being approximated by some  $F_c$  to cancel out the leading order error term in (36). This can be achieved, for example, by matching the resulting impedance function to the exact one for a particular choice of direction of  $\mathbf{q}$ , just as was done in the two-dimensional case. Matching the impedance function for  $q_1 = 0$ , we arrive at

$$F_c(\lambda) = \frac{h_\perp \sqrt{3}}{2 \arccos\left(1 - \frac{3}{8} h_\perp^2 \lambda\right)}. \quad (38)$$

With this choice of  $F_c$ , we have

$$F_c \left[ \frac{4}{3h_\perp^2} \left\{ 3 - \cos(q_1 h_\perp) - 2 \cos\left(\frac{q_1 h_\perp}{2}\right) \cos\left(\frac{q_2 h_\perp \sqrt{3}}{2}\right) \right\} \right] = F(|\mathbf{q}|) + O(h_\perp^4), \quad (39)$$

for all choices of  $\mathbf{q}$ , with the error term vanishing identically for all  $\mathbf{q} = (0, q)$ . Finally, constructing an optimal grid from the rational approximant  $F_n$  of the modified impedance function  $F_c$  on the spectral interval  $\lambda \in [\lambda_{\min}, \lambda_{\max}]$ , with  $\lambda_{\min} = O(1)$  and  $\lambda_{\max} = O(h_\perp^{-2})$ , we will resolve the solution at  $z = 0$  with  $O(h_\perp^4)$  accuracy, provided the value of  $n$  is chosen to be sufficiently big. While the obtained accuracy is no longer spectral-like, as in the case of one-dimensional problems, it nevertheless is of higher order than the expected second-order accuracy of such a 9-point stencil in three dimensions.

We performed numerical tests, of the proposed method by solving the discretized version of the problem (32) and (33) with the help of the diagonally preconditioned conjugate gradient method, choosing  $L_x = \pi$  and  $L_y = \frac{115}{200} \pi \sqrt{3}$  with  $h_\perp = \frac{\pi}{200}$ . We used two different optimal rational approximants for  $F_c$  in (38): one with  $n = 8$  optimized on the spectral interval  $\lambda \in [1, 10^3]$ , and the other with  $n = 14$  optimized on the spectral interval  $\lambda \in [3 \times 10^{-1}, 3 \times 10^2]$ . The results for several choices of  $\mathbf{q}$  are shown in Fig. 7. One can see that, as  $|\mathbf{q}|$  is decreased, the accuracy of the solution quickly reaches the resolution limit of  $3.2 \times 10^{-7}$  for the  $n = 8$  optimal grid, and stays low for all smaller wave vectors in the problem. The performance of this grids is essentially as good as that of the one-dimensional compensated optimal grid constructed earlier (see Section 3.3). On the other hand, in the case of the  $n = 14$  optimal grid the error does not quite reach the resolution limit of  $1.6 \times 10^{-12}$  for most of the wave vectors. Nevertheless, in this case the error behaves as  $O(|\mathbf{q}|^4)$ , and rapidly decreases, as expected.

#### 4.2. Compensation on anisotropy-adjusted square grids

Another approach to anisotropy reduction is to modify the finite-difference stencil used to discretize the problem in the  $xy$ -plane to achieve higher degree of isotropy for the discrete problem. Note that this is different than using higher-order discretization for spatial derivatives, since the resulting stencil may still remain  $O(h_\perp^2)$  accurate.

Let us illustrate this approach for the boundary-value problem given by (32) and (33). We want to discretize the transverse Laplacian  $\Delta_\perp$  on a square grid with step size  $h_\perp$ , using as compact a stencil as possible. As was already pointed out, the most natural choice of a 5-point stencil would not work because the anisotropy it produces appears in the second order in  $h_\perp$ . So, instead, we consider a centered 9-point stencil involving nearest and next-to-nearest neighbors of each grid point (see Fig. 6(b)). It turns out that it is possible to choose (uniquely) the relative weights of different points in the stencil in such a way that the obtained discretization of  $\Delta_\perp$  is consistent up to  $O(h_\perp^2)$  and at the same time has anisotropy appearing only

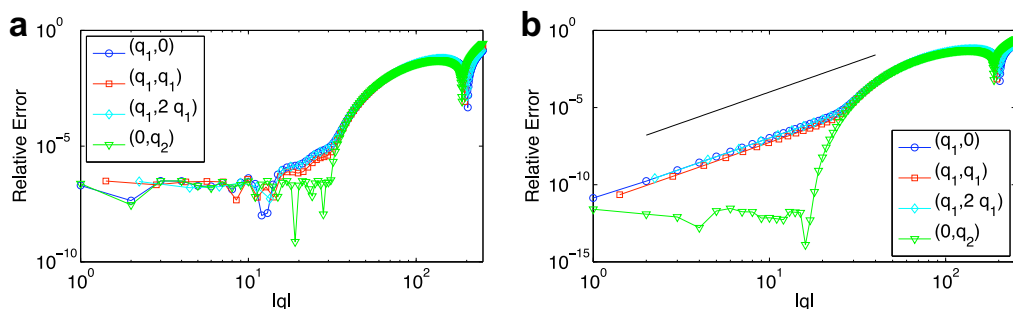
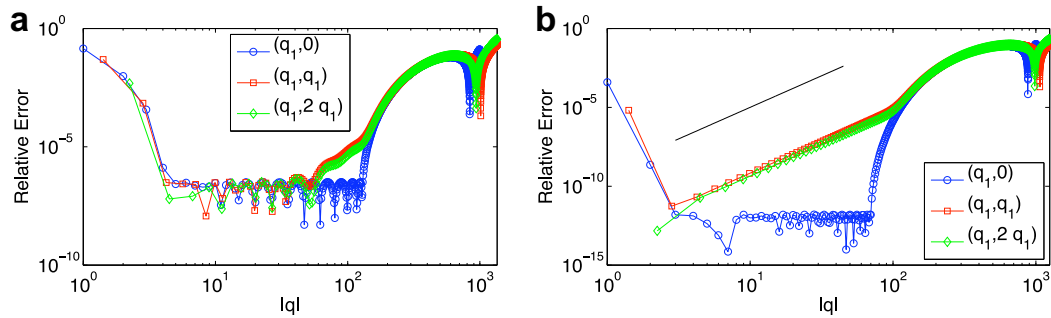


Fig. 7. The  $L^\infty$  norm of the relative error of the numerical solution of (32) and (33) obtained, using hexagonal grids in the  $xy$ -plane and compensated optimal grids with  $n = 8$  in (a) and  $n = 14$  in (b) (see text for complete details). In (b), the straight line indicates the  $O(|\mathbf{q}|^4)$  dependence.



**Fig. 8.** The  $L^\infty$  norm of the relative error of the numerical solution of (32) and (33) obtained, using anisotropy-adjusted square grids in the  $xy$ -plane and compensated optimal grids with  $n = 8$  in (a) and  $n = 14$  in (b) (see text for complete details). In (b), the straight line indicates the  $O(|\mathbf{q}|^4)$  dependence.

in  $O(h_\perp^4)$ . Denoting by  $i$  and  $j$  the cartesian indices of the points on the square grid in the  $xy$ -plane and by  $k$  the index of the staggered grid in the  $z$ -direction, we obtain

$$\Delta_\perp u^k(x_i, y_j) \approx \frac{1}{6h_\perp^2} \left\{ 4(u_{i+1,j}^k + u_{i-1,j}^k + u_{i,j+1}^k + u_{i,j-1}^k) + u_{i+1,j+1}^k + u_{i+1,j-1}^k + u_{i-1,j+1}^k + u_{i-1,j-1}^k - 20u_{i,j}^k \right\}, \quad (40)$$

where now  $x_i = ih_\perp$  and  $y_j = jh_\perp$ . With this choice of the discretization we have

$$e^{-iq_1x - iq_2y} \Delta_\perp e^{iq_1x + iq_2y} \approx \frac{2}{3h_\perp^2} \{ 2 \cos(q_2h_\perp) + \cos(q_1h_\perp)(\cos(q_2h_\perp) + 2) - 5 \} = -|\mathbf{q}|^2 + \frac{1}{12} h_\perp^2 |\mathbf{q}|^4 + O(h_\perp^4), \quad (41)$$

similarly to (36). Hence, using the discretization of (40) in place of the 7-point stencil in a suitably modified version of (34) and (35), we find the solution to be

$$u(x_i, y_j, 0) \approx \cos q_1 x_i \cos q_2 y_j \times F_n \left[ \frac{2}{3h_\perp^2} \{ 5 - 2 \cos(q_2h_\perp) - \cos(q_1h_\perp)(\cos(q_2h_\perp) + 2) \} \right], \quad (42)$$

where, again,  $F_n$  is the impedance function of the staggered grid. We now note that for  $q_2 = 0$  the solution in (42) reduces to

$$u(x_i, y_j, 0) \approx F_n [2h_\perp^{-2} (1 - \cos q_1 h_\perp)] \cos q_1 x_i, \quad (43)$$

an expression which coincides with (18) obtained for the one-dimensional problem. Therefore, approximating by  $F_n$  the impedance function  $F_c$  from (20), we have  $u(x_i, y_j, 0) \approx F(q_1^2) \cos q_1 x_i$ , and, moreover, for all  $\mathbf{q}$

$$u(x_i, y_j, 0) \approx F(|\mathbf{q}|) \cos q_1 x_i \cos q_2 y_j + O(h_\perp^4). \quad (44)$$

In other words, we obtain a result similar to the one in the case of hexagonal lattices with the 7-point stencil, i.e., the solution of the discrete problem is approximating the exact solution of the boundary-value problem as good as the rational function  $F_n$  approximates the modified impedance function  $F_c$  given by (20), and the solution is  $O(h_\perp^4)$  accurate for all wave vectors at sufficiently large values of  $n$ . Curiously enough, the obtained 9-point stencil turns out to coincide with the fourth-order accurate stencil for discretizing the Laplace's equation in the plane, see e.g., Refs. [30,31]. We note that the compensated optimal grid in this case coincides with the one already constructed for the two-dimensional problem in Section 3.2.

The results of the numerical studies analogous to those of Section 4.1 are presented in Fig. 8. In (32) and (33) we chose  $L_x = L_y = \pi$  and discretized the problem with  $h_\perp = \frac{\pi}{1000}$ , using the compensated optimal grids constructed earlier in Section 3.3 with  $n = 8$  and  $n = 14$ . The obtained results essentially coincide with those obtained, using the method of Section 4.1.

### 5. Application to cell signaling

We now demonstrate the utility of the methods developed in the preceding sections by applying them to a problem arising in cell signaling. The problem under consideration involves an interaction of a positive feedback loop established through receptor signaling by ligand-induced ligand release mechanism [22,4,24,25] with an imposed morphogen gradient. A morphogen is a diffusible chemical that can induce multiple cellular responses depending on its concentration during development [8].

For concreteness, consider the following idealized situation in which a particular cell in a flat epithelium surrounded by semi-infinite extracellular medium (see Section 2) is emitting a morphogen molecule at the rate of  $Q_w$  molecules in a unit of time. Neglecting, for simplicity, the recapture of the morphogen by the cells and assuming that the size of the cell is negligible on the length scale of the problem, the concentration  $w$  of the morphogen molecule satisfies the following equation

$$w_t = D_w \Delta w \quad \text{for } z > 0, \quad -D_w w_z = Q_w \delta(x) \delta(y) \quad \text{at } z = 0, \quad (45)$$

where we placed the emitting cell at the origin. Here  $\delta(x)$  denotes Dirac delta-function and  $D_w$  is the morphogen diffusion constant.

Let us now suppose that the morphogen molecule reversibly binds to its own receptor to form a morphogen-receptor complex, which is required to activate signaling through the positive feedback loop. Assuming fast equilibration kinetics and that the morphogen-sensing receptors are in excess, we may conclude that the density of morphogen-receptor complexes  $w^*$  is proportional to morphogen concentration at the cell surface:

$$w^* = \frac{k_{w,on}r_w}{k_{w,off}}w \quad \text{at } z = 0, \tag{46}$$

where  $k_{w,on}r_w$  is the morphogen-receptor binding rate times the number of receptors per unit area and  $k_{w,off}$  is the morphogen-receptor dissociation constant.

We now assume that ligand release depends on the product of concentrations of the inductive signal (the morphogen) and the induced ligand. This algebraic expression can be viewed as an approximation of the AND logic commonly encountered in developmental gene regulatory networks [32]. With this in mind, the input to the signaling cascade in the secretion rate (the argument of the Hill function in (4)) should now be taken to be proportional to the cell surface density of ligand-receptor and morphogen-receptor complexes:

$$g_s = -\frac{k_{s,ec}k_{s,on}r_s s(t, x, y, 0)}{k_{s,off} + k_{s,ec}} + \frac{\bar{g}_s c^v}{c_0^v + c^v}, \quad c = \alpha_{sw} S^* w^*, \tag{47}$$

where, as before, we assumed fast equilibration of the binding kinetics.

In the case of stationary signaling profiles, which are of particular interest to development, the problem under consideration can be further simplified by noting that the steady solution of (45) at the epithelium surface is  $w = (Q_w/2\pi D_w)(x^2 + y^2)^{-1/2}$ . Introducing the quantities

$$u = \frac{k_{s,on}k_{s,ec}r_s}{\bar{g}_s(k_{s,off} + k_{s,ec})}s, \quad \kappa = \frac{2\pi D_w D_s k_{w,off}(k_{s,off} + k_{s,ec})c_0}{\alpha_{sw}\bar{g}_s Q_w k_{w,on}k_{s,on}r_s r_w}, \tag{48}$$

and scaling length with  $L = D_s(k_{s,off} + k_{s,ec})/(k_{s,ec}k_{s,on}r_s)$ , we arrive at (6) with

$$f(x, y, \bar{u}) = -\bar{u} + \frac{\bar{u}^v}{\kappa^v(x^2 + y^2)^{v/2} + \bar{u}^v}. \tag{49}$$

We have simulated the problem in (6) and (49) with  $v = 2$  and  $\kappa = 0.15$  on a square  $(x, y) \in [-L, L] \times [-L, L]$  with Dirichlet boundary conditions, using a relaxation algorithm similar to the one described in Section 3.4 (for simplicity, Dirichlet boundary conditions are chosen to avoid the issue of treating the spatial average of the solution). In practice, the problem was solved on a hexagonal grid covering the first quadrant with Neumann boundary conditions at  $x = 0$  or  $y = 0$ , and Dirichlet boundary conditions at  $x = L_x$  or  $y = L_y$ , with  $L_x, L_y$  chosen sufficiently close to  $L = 15$  in a way compatible with the lattice. We used the suitably rescaled  $n = 14$  compensated optimal grid obtained in Section 4 and varied  $h_\perp$  in the range  $h_\perp = 0.1-1$ . The profile of the solution for  $h_\perp = 0.25$  is shown in Fig. 9(a). It has the expected bell-shaped profile, with high signaling restricted to a small neighborhood of the cell emitting the morphogen. Also, quite expectedly, we found that the region of high signaling grows upon decrease of  $\kappa$  (corresponding to increase in  $Q_w$ ), and shrinks with increase of  $\kappa$ , until at some critical value of  $\kappa$  the solution disappears altogether. This signifies a region of bistability, since the problem always has  $\bar{u} = 0$  as the trivial solution.

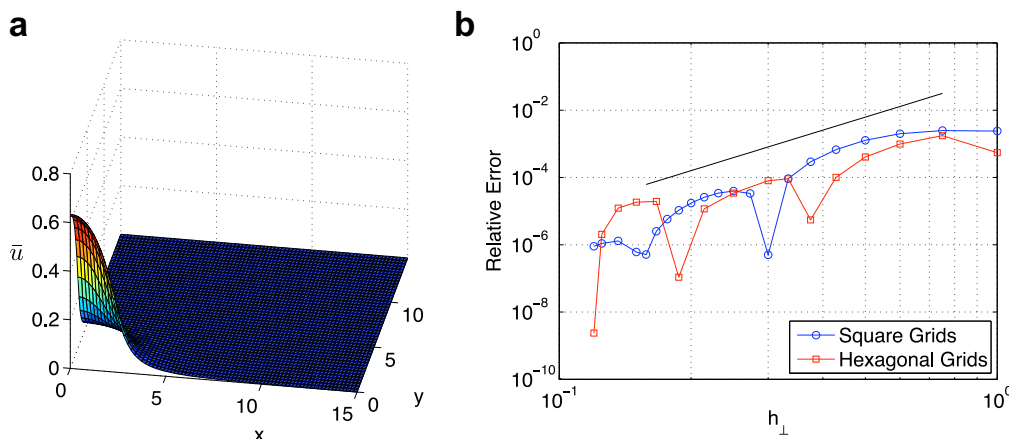


**Fig. 9.** (a) The profile of the solution of (6) and (49) obtained using the  $n = 14$  compensated optimal grid of Section 4 on a hexagonal lattice with  $h_\perp = 0.25$ ,  $L_x = 60h_\perp$ ,  $L_y = 68h_\perp\sqrt{3}/2$ . (b) The relative error of  $\bar{u}(0, 0)$  obtained using the  $n = 14$  compensated optimal grids of Section 4 for hexagonal and anisotropy-adjusted square lattices. In (b), the straight line indicates the  $O(h_\perp^4)$  dependence.

We have also performed convergence studies of the solution to assess the accuracy and efficiency of the method. As the indicator, we chose the maximum value of  $\bar{u}$  in the computational domain, which is attained at the origin. The results of these studies for both the hexagonal and anisotropy-adjusted square lattices combined with their corresponding  $n = 14$  compensated optimal grids obtained in Section 4 are presented in Fig. 9(b). As expected, both lattices produce solutions that are fourth-order accurate in  $h_{\perp}$ .

## 6. Conclusions

To conclude, we have developed an extension of the method of optimal grids which takes into account the additional source of numerical error introduced by spatial discretization of the elliptic differential operator on the domain boundary. We showed that for a number of boundary discretizations one can actually compensate this error by choosing a suitably modified impedance function to be approximated by a rational function generating the steps of the grid. This is done in an optimal way in the sense of the minimax approximation of the relative error on the spectral interval which covers most of the wave vectors of the discrete problem. We note that, in some sense, the compensated optimal grids provide the best way to match the discrete and continuous boundary value problems in the sense of achieving the best accuracy for the boundary data using the smallest discretization grid possible.

We have demonstrated that for the Laplace's equation in the upper half-plane discretized uniformly along the boundary one can increase the accuracy of the optimal grid method from second-order to essentially spectral accuracy by simply changing the impedance function being approximated. This is because in the case of two-dimensional problems (hence one-dimensional boundary) the eigenvalues of the discrete DtN map are ordered, while the eigenfunctions of the continuous and discrete problems coincide. Therefore, applying a suitable transformation one can map the impedance function of the discrete problem to that of the continuous problem exactly. While this example is more of a methodological significance, it shows an interesting relation of the method of compensated optimal grids to the fast Fourier transform (FFT)-based methods. Indeed, according to the error estimate in (19), which is expected to remain qualitatively valid in our case, too, the method of compensated optimal grids requires that the size of the optimal grid be on the order of  $\ln m$ , where  $m$  is the number of discretization nodes on the boundary, thus making the size of the full two-dimensional grid  $O(m \ln m)$ . As a result, for example, a relaxation algorithm like the one used in Section 5 would require a comparable amount of computations to arrive at the result as an FFT-based algorithm.

On the other hand, for three-dimensional isotropic problems (as in the case of the Laplace's equation considered here) the mapping between the continuous and the discrete impedance function is no longer possible, since the isotropy is lost on the discrete level. Nevertheless, as we showed in this paper, by a particular choice of the discretization of the boundary (e.g. by using hexagonal or anisotropy-compensated square grids for the Laplace's equation) it is possible to eliminate the effect of the discretization error at least at the lowest order in  $h_{\perp}$ . As a result, for these lattices the method provides an unexpectedly high order of accuracy, e.g.  $O(h_{\perp}^4)$  instead of the usual  $O(h_{\perp}^2)$  order for the Laplace's equation in three dimensions.

The obtained finite-difference discretizations present three main advantages for studying boundary-value problems with nonlinear boundary conditions, such as those which arise in the problems of cell-to-cell communication considered here. First, these schemes are very easy to implement and can be readily incorporated into existing codes, the only programming effort is involved in obtaining the optimal grid steps. Second, the resulting schemes involve sparse matrices and, therefore, easily lend themselves to Newton-like methods, etc. Third, for multiscale problems involving localized isolated boundary sources a multi-grid approach using patches of uniform grids in the plane coupled to the compensated optimal grid in the normal direction should produce accurate discretizations without the need of too many discretization points. In this case one should also be able to apply these methods to domains with general boundaries. All these features may make the compensated optimal grid method superior to the conventional FFT-based methods for the considered class of problems. Let us also point out that time-dependent problems can be treated equally well, using our discretization approach, since the obtained grids are consistent to  $O(h_{\perp}^2)$  with the parabolic problem in the Fourier-Laplace transform space [33].

## Acknowledgments

One of the authors (CBM) would like to acknowledge multiple valuable discussions with V. Druskin. This work was supported by NIH via Grant R01 GM076690.

## References

- [1] A. DeSimone, R.V. Kohn, S. Müller, F. Otto, Magnetic microstructures – a paradigm of multiscale problems, in: ICIAM 99 (Edinburgh), Oxford University Press, 2000, pp. 175–190.
- [2] B.S. Kerner, V.V. Osipov, Autosolitons, Kluwer, Dordrecht, 1994.
- [3] B. Pando, J.B. Pearson, S. Ponce-Dawson, Sheet excitability and nonlinear wave propagation, Phys. Rev. Lett. 91 (2003) 258101.
- [4] M. Pfißl, C.B. Muratov, S.Y. Shvartsman, Long-range signal transmission in autocrine relays, Biophys. J. 84 (2003) 883–896.
- [5] N. Mazouz, G. Flatgen, K. Krischer, Tuning the range of spatial coupling in electrochemical systems: from local via nonlocal to global coupling, Phys. Rev. E 55 (1997) 2260–2266.
- [6] A. Birzu, B.J. Green, N.I. Jaeger, J.L. Hudson, Spatiotemporal patterns during electrodisolution of a metal ring: three-dimensional simulations, J. Electroanal. Chem. 504 (2001) 126–136.
- [7] D. Tseluiko, D. Papageorgiou, Nonlinear dynamics of electrified thin liquid films, SIAM J. Appl. Math. 67 (2007) 1310–1329.

- [8] G.T. Reeves, C.B. Muratov, T. Schüpbach, S.Y. Shvartsman, Quantitative models of developmental pattern formation, *Dev. Cell* 11 (2006) 289–300.
- [9] S.V. Tsynkov, Numerical solution of problems on unbounded domains. A review, *Appl. Numer. Math.* 27 (1998) 465–532.
- [10] Z. Gimbutas, L. Greengard, M. Minion, Coulomb interactions on planar structures: inverting the square root of the Laplacian, *SIAM J. Sci. Comput.* 22 (2001) 2093–2108.
- [11] B. Fornberg, *A practical guide to pseudospectral methods*, Cambridge University Press, Cambridge, 1996.
- [12] L.A. Ying, *Infinite element methods*, Peking University Press, Beijing, 1995. Chinese Edition.
- [13] F. Alouges, J. Laminie, S.M. Meffire, Exponential meshes and three-dimensional computation of a magnetic field, *Numer. Meth. Part. Differ. Equat.* 19 (2003) 595–637.
- [14] M.N. Guddati, J.L. Tassoulas, Continued-fraction absorbing boundary conditions for the wave equation, *J. Comput. Acoust.* 8 (2000) 139–156.
- [15] V. Druskin, Spectrally optimal finite-difference grids in unbounded domains, *Schlumberger-Doll Research Notes* (1997) EMG-002-97-22, 1997.
- [16] D. Ingerman, V. Druskin, L. Knizhnerman, Optimal finite-difference grids and rational approximations of the square root: I. Elliptic problems, *Commun. Pure Appl. Math.* 53 (2000) 1039–1066.
- [17] V. Druskin, L. Knizhnerman, Gaussian spectral rules for the three-point second differences: I. A two-point positive definite problem in a semiinfinite domain, *SIAM J. Numer. Anal.* 37 (1999) 403–422.
- [18] S. Asvadurov, V. Druskin, L. Knizhnerman, Application of the difference Gaussian rules to solution of hyperbolic problems, *J. Comput. Phys.* 158 (2000) 116–135.
- [19] S. Asvadurov, V. Druskin, L. Knizhnerman, Application of the difference Gaussian rules to solution of hyperbolic problems. II. Global expansion, *J. Comput. Phys.* 175 (2002) 24–49.
- [20] C.B. Muratov, V.V. Osipov, Optimal grid-based methods for thin film micromagnetics simulations, *J. Comput. Phys.* 216 (2006) 637–653.
- [21] N. Yakoby, J. Lembong, T. Schüpbach, S.Y. Shvartsman, *Drosophila* eggshell is patterned by sequential action of feedforward and feedback loops, *Development* 135 (2008) 343–351.
- [22] M. Freeman, J.B. Gurdon, Regulatory principles in developmental signaling, *Annu. Rev. Cell Dev. Biol.* 18 (2002) 515–539.
- [23] M. Freeman, Feedback control of intercellular signalling in development, *Nature* 408 (2000) 313–319.
- [24] M. Přibyl, C.B. Muratov, S.Y. Shvartsman, Discrete models of autocrine cell communication in epithelial layers, *Biophys. J.* 84 (2003) 3624–3635.
- [25] C.B. Muratov, S.Y. Shvartsman, Signal propagation and failure in discrete autocrine relays, *Phys. Rev. Lett.* 93 (2004) 118101.
- [26] M.E. Taylor, *Partial Differential Equations II: Qualitative Studies of Linear Equations*, Springer-Verlag, Berlin, 1996.
- [27] E.W. Cheney, *Introduction to Approximation Theory*, second ed., AMS, Providence, RI, 1999.
- [28] J.F. Toland, The Peierls-Nabarro and Benjamin-Ono equations, *J. Funct. Anal.* 145 (1997) 136–150.
- [29] R. Peierls, The size of a dislocation, *Proc. Phys. Soc.* 52 (1940) 34–37.
- [30] J.B. Rosser, Nine-point difference solutions for Poisson's equation, *Comp. Math. Appl.* 1 (1975) 351–460.
- [31] J.C. Strikwerda, *Finite Difference Schemes and Partial Differential Equations*, Wadsworth and Brooks/Cole Advanced Books and Software, Pacific Grove, CA, 1989.
- [32] S.B.T. De-Leon, E.H. Davidson, Gene regulation: gene control network in development, *Annu. Rev. Biophys. Biomol. Struct.* 36 (2007) 191–212.
- [33] F. Posta, S.Y. Shvartsman, C.B. Muratov, in preparation.